# CD45 regulates retention, motility, and numbers of hematopoietic progenitors, and affects osteoclast remodeling of metaphyseal trabecules

Shoham Shivtiel,[1] Orit Kollet,[1] Kfir Lapid,[1] Amir Schajnovitz,[1] Polina Goichberg,[1] Alexander Kalinkovich,[1] Elias Shezen,[1] Melania Tesio,[1] Neta Netzer,[1] Isabelle Petit,[1] Amnon Sharir,[2,3] and Tsvee Lapidot[1]

[1]Department of Immunology and [2]Molecular Genetics, Weizmann Institute of Science, Rehovot 76100, Israel
[3]The Laboratory of Musculoskeletal Biomechanics and Applied Anatomy, Koret School of Veterinary Medicine, Hebrew University of Jerusalem, Rehovot 76100, Israel

**The CD45 phosphatase is uniquely expressed by all leukocytes, but its role in regulating hematopoietic progenitors is poorly understood. We show that enhanced CD45 expression on bone marrow (BM) leukocytes correlates with increased cell motility in response to stress signals. Moreover, immature CD45 knockout (KO) cells showed defective motility, including reduced homing (both steady state and in response to stromal-derived factor 1) and reduced granulocyte colony-stimulating factor mobilization. These defects were associated with increased cell adhesion mediated by reduced matrix metalloproteinase 9 secretion and imbalanced Src kinase activity. Poor mobilization of CD45KO progenitors by the receptor activator of nuclear factor κB ligand, and impaired modulation of the endosteal components osteopontin and stem cell factor, suggested defective osteoclast function. Indeed, CD45KO osteoclasts exhibited impaired bone remodeling and abnormal morphology, which we attributed to defective cell fusion and Src function. This led to irregular distribution of metaphyseal bone trabecules, a region enriched with stem cell niches. Consequently, CD45KO mice had less primitive cells in the BM and increased numbers of these cells in the spleen, yet with reduced homing and repopulation potential. Uncoupling environmental and intrinsic defects in chimeric mice, we demonstrated that CD45 regulates progenitor movement and retention by influencing both the hematopoietic and nonhematopoietic compartments.**

CORRESPONDENCE
Tsvee Lapidot:
Tsvee.Lapidot@weizmann.ac.il

Abbreviations used: CFC, colony-forming cell; DC-STAMP, DC-specific transmembrane protein; Erk, extracellular signal-regulated kinase; FN, fibronectin; MMP, matrix metalloproteinase; MNC, mononuclear cell; PB, peripheral blood; PYD, pyridinoline; RANKL, receptor activator of NF-κB ligand; SCF, stem cell factor; SDF-1, stromal-derived factor 1; SKL, Sca-1$^+$/c-Kit$^+$/Lin−; Tb.N, trabecular number; TRAP, tartrate-resistant acid phosphatase; WBC, white blood cell.

Hematopoiesis is associated with primitive stem cell proliferation and differentiation leading to the production of maturing cells in the BM, followed by their continuous release to the circulation. One of the basic characteristics of immature and maturing hematopoietic cells is their unique ability to migrate between different organs, particularly in and out of the BM, as manifested during both homeostasis and stress conditions (1).

Egress of progenitors and maturing cells from the BM is accelerated during alarm situations that are associated with urgent needs to rapidly cope with physiological demands, such as host defense and repair. This process is termed "mobilization," and it is induced by different stimulations, including cytokines and inflammatory and chemotherapeutic agents. The cytokine G-CSF is clinically used to induce stem cell mobilization as a source harvested for BM transplantation protocols (2–5). The migration of circulating progenitor cells back to their BM is termed "homing," a multistep process in which the immature cells actively cross the endothelium barrier between the circulation and the BM compartment. Homing has physiological roles in adult BM homeostasis and in the course of BM repopulation during stem cell transplantations in patients (6).

Both mobilization and homing require active navigation and use partially overlapping



The Rockefeller University Press $30.00
J. Exp. Med. Vol. 205 No. 10 2381-2395
www.jem.org/cgi/doi/10.1084/jem.20080072

mechanisms (7). These complex processes involve an interplay between cytokines, chemokines, adhesion molecules, and proteolytic enzymes. Adhesion molecules, including members of the β1 and β2 integrins, are crucial for undifferentiated cell retention in their BM niches, maintaining the stem cell pool and function. Breakdown of this anchorage is essential for progenitor cell release (3, 8). Proliferation and migration of primitive cells are regulated by various cytokines and chemokines such as stromal-derived factor 1 (SDF 1; also termed CXCL12), its receptor CXCR4, and the cytokine stem cell factor (SCF) (7, 9–11). Proteolytic enzymes, especially metalloproteinases (MMPs), play central roles in various steps of stem cell mobilization and homing. These enzymes cleave different adhesion interactions, extracellular matrix components, and cytokines, which further facilitate cell egress through the mechanical and endothelial barriers (9, 12–15). Recently, we suggested a new regulator of progenitor cell mobilization by demonstrating that bone-degrading osteoclasts play a major role in homeostatic release and selective stress-induced progenitor cell mobilization (16). These hematopoietic-derived multinucleated, fused giant cells are involved in bone remodeling processes. Different players regulate osteoclast development, recruitment, and function in their bone resorbing sites. The seven-transmembrane-region receptor DC-specific transmembrane protein (DC-STAMP) was shown to mediate cell–cell fusion of osteoclast precursors and the assembly of multinucleated cells (17). In addition, Src kinases were shown to be involved in sealing zone formation (18), and osteoclast motility is regulated by MMP expression and secretion (for review see reference 19). The role of osteoclasts in progenitor cell mobilization involves cleavage of endosteal components such as SDF-1, SCF, and osteopontin, which are regulators of stem cell anchorage and retention (16). Previous studies have introduced the linkage between bone remodeling, regulation of hematopoiesis, and the dynamic nature of BM stem cell niches (5). However, in spite of extensive experiments, the exact mechanisms and regulators underlying the migration, localization, and retention of hematopoietic progenitor cells have not been fully elucidated.

All leukocytes, including hematopoietic stem and progenitor cell populations, are characterized by unique cell surface expression of CD45. CD45 is a transmembrane protein tyrosine phosphatase. It dephosphorylates different sites on Src family kinases, and can serve as both a positive and negative regulator in a cell type– and context-dependent manner (20, 21). CD45 was shown to regulate different stages of lymphocyte maturation (22), especially their activation and proliferation (23, 24). However, its potential role in the function of earlier, undifferentiated hematopoietic progenitor cells was not identified. The distinctive expression of CD45 led us to postulate that this phosphatase may regulate fundamental processes of immature hematopoietic cells. Our results show that CD45 has multiple roles in regulating the cell autonomous motility of progenitor cells and retention of these cells in the BM, as well as osteoclast-mediated remodeling of the metaphyseal bone trabecules.

## RESULTS

### CD45 expression is dynamically modulated by stress signals

To evaluate the potential involvement of the panleukocyte CD45 phosphatase in the mobilization and recruitment of immature cells, we tested its expression levels in response to stress signals. G-CSF stimulations significantly increased expression of CD45 by mononuclear cells (MNCs) in the BM (Fig. 1, A and B). CD45 up-regulation in the BM was observed in mature leukocytes such as lymphoid $CD4^+$ and myeloid $CD11b^+$ cells and, moreover, in immature hematopoietic c-$Kit^+$ progenitors (Fig. 1 C). Similar results were obtained when mice were stimulated with LPS, mimicking bacterial-induced inflammation (Fig. 1 D). This increase in CD45 expression on BM leukocytes correlated with their release to the circulation during G-CSF mobilization (Fig. 1 E). CD45 expression was elevated by 1.3-fold on day 1 and by 1.5-fold on day 3, reaching 1.6-fold on day 5, when both cell mobilization and CD45 levels gained their peak values. Hence, G-CSF treatment led to a gradual increase in the expression of CD45 on BM cells before their egress. Interestingly, we observed in the circulation a reduction in CD45 expression on mobilized cells compared with untreated blood cells (Fig. 1, A and B). These results reveal that CD45 expression is modulated during cell mobilization, suggesting that dynamic CD45 expression participates in egress from the BM in response to different stress signals.

### Impaired progenitor expansion and reduced mobilization in mice lacking CD45

To further elucidate the role of CD45 in cell egress, the model of CD45KO mice was used. We tested the potential of CD45KO cells to egress from the BM under steady-state conditions and in response to G-CSF stimulations. Importantly, differential BM cell count demonstrated no major differences in the composition of mature cells obtained from WT versus CD45KO mice (unpublished data). As shown by others (23), we also did not detect substantial differences in the total numbers of circulating white blood cells (WBCs) in untreated CD45KO and WT mice (Fig. 1 E). However, G-CSF stimulations in CD45KO mice resulted in a delayed and reduced response. A suboptimal protocol of G-CSF, administrated for 3 d only compared with the optimal protocol of 5 d, was tested. After 3 d of injections, we documented a significant reduction (∼50%) in the number of mobilized WBCs in the circulation of CD45KO mice compared with their WT counterparts. Of note, in this suboptimal protocol the numbers of mobilized WT cells were already very high, near their peak levels, as documented after 5 d of stimulations (Fig. 1 E). Notably, mobilization of immature CD45KO progenitor cells was also significantly impaired, which is reflected by the frequency of circulating colony-forming cells (CFCs) (Fig. 1 F). Moreover, we found in the peripheral blood (PB) of CD45KO mice lower numbers of primitive Sca-$1^+$/c-$Kit^+$/$Lin^-$ (SKL) cells (a rare population shown to contain most of the stem cell activity) after 3 d of G-CSF injections (Fig. 1, G and I). Progenitor cell proliferation within the BM reservoir is a prerequisite process for cell egress and

G-CSF–induced mobilization (25). We therefore examined the ability of primitive BM cells to expand in vivo in response to G-CSF stimulations. After 3 d of G-CSF treatment, CFCs in the WT BM increased their numbers by 1.5-fold (Fig. 1 H). However, in the CD45KO mice, we first observed that untreated mice have a priori lower numbers of CFCs in the BM. Of note, CD45KO CFCs expanded to a lower extent in response to G-CSF stimulation for 3 d, a time frame

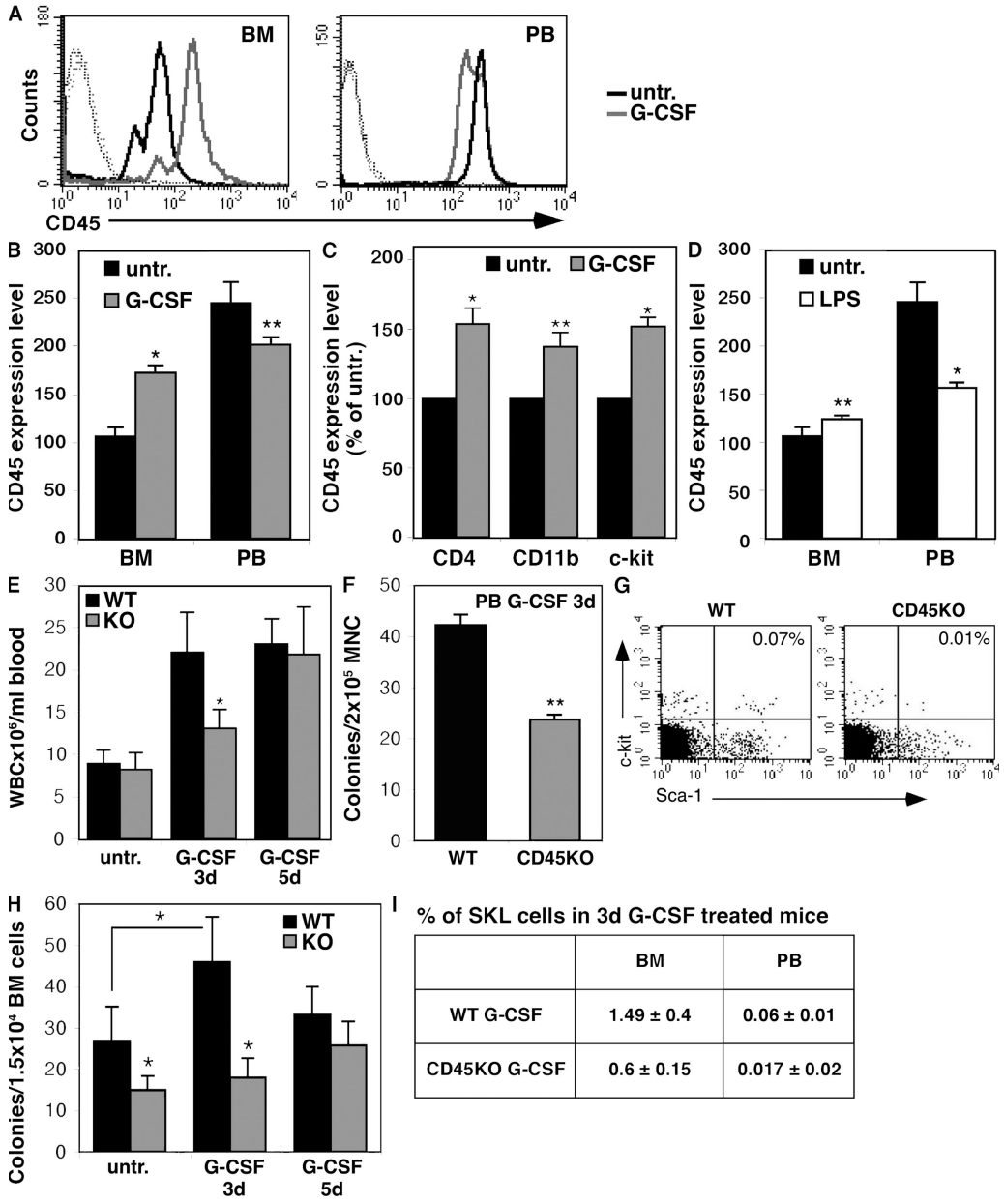


| | BM | PB |
|---|---|---|
| WT G-CSF | 1.49 ± 0.4 | 0.06 ± 0.01 |
| CD45KO G-CSF | 0.6 ± 0.15 | 0.017 ± 0.02 |

**Figure 1. CD45 expression is modulated and essential for cell mobilization.** (A–D) CD45 expression. WT mice were untreated (untr.), or were treated with G-CSF for 5 consecutive days (A–C) or with a single injection of LPS (D). MNCs from BM and PB samples were examined for their CD45 expression by FACS. A representative histogram of CD45 levels is shown in A. Isotype control staining (dotted lines), untreated cells (black line), and cells after 5 d of G-CSF stimulations (gray line) are shown. A summary of four independent experiments is shown for G-CSF (B and C) and LPS (D). CD45 expression (presented as a geometric mean value) on different sorted subpopulations after G-CSF stimulations for 5 d is shown in C. (E) In vivo mobilization. WT and CD45KO mice were injected with G-CSF for 3 and 5 d or were left untreated. Total numbers of viable circulating WBCs were evaluated. (F) Frequency of CFCs in the PB of 3 d of G-CSF–treated mice. The data summarize three independent experiments (±SD). (G) Representative FACS analysis of MNCs derived from the PB after 3 d of G-CSF stimulations. Indicated values represent the percentage of SKL primitive cells in PB MNCs. One representative figure out of five independent experiments is shown. (H) Kinetics of the increased CFC numbers in the BM of G-CSF–treated WT and CD45KO mice. Numbers of colonies were evaluated in untreated mice or after G-CSF administration for 3 and 5 d. Bars represent at least three mice in each group, showing mean ± SD. *, $P < 0.01$; **, $P < 0.05$. (I) Table summarizing the percentage of SKL cells out of BM and PB MNCs in WT or CD45KO mice after G-CSF treatment for 3 d.

in which the number of immature progenitors in the WT BM has already reached a plateau (Fig. 1 H). Importantly, reduced numbers of primitive CD45KO SKL cells were also documented in the BM after G-CSF stimulation compared with their WT counterparts (Fig. 1 I).

### Reduced motility and response to SDF-1 are associated with impaired homing of CD45KO progenitors

The lower numbers of progenitors in the CD45KO BM may lead to their reduced appearance in the PB after G-CSF treatment. To examine if CD45 is directly involved in progenitor cell motility, we isolated BM subpopulations from CD45KO mice and evaluated their spontaneous and SDF-1–induced migration potential. The migration of CD45KO MNCs was significantly reduced compared with WT cells (Fig. 2 A), including both spontaneous as well as SDF-1–directional migration. Of note, no differences were observed in the expression of CXCR4, the receptor for SDF-1 (unpublished data). MNCs isolated from the BM of G-CSF–treated mice exhibited higher motility compared with untreated cells (Fig. 2 A). This high motility of G-CSF–treated WT cells correlated with their increased CD45 expression levels (Fig. 1, A and B). However, reduced migration was observed in cells obtained from CD45KO mice despite G-CSF treatment. Importantly, although normal mobilization levels were observed after 5 d of G-CSF administration, CD45KO BM MNCs still demonstrated reduced spontaneous and SDF-1 migration compared with their WT counterparts (Fig. 2 A). When CD45KO BM MNCs were allowed to migrate through a fibronectin (FN)-coated barrier, stronger reductions in their migration were observed (Fig. 2 B). These results suggest that together with their intrinsic defects in cell motility, CD45KO cells predominantly have an impaired ability to cross extracellular matrix barriers. This notion was further evident in vivo, as CD45KO MNCs showed reduced homing compared with their WT counterparts (Fig. 2 C). Next, we examined the motility potential of sorted representative subpopulations that strongly respond to G-CSF: $CD11b^+$ monocytes and c-$Kit^+$ enriched progenitor cells. These cell fractions were isolated from the BM of WT and CD45KO mice untreated or treated with G-CSF for 5 d. As observed with the MNC population, CD45KO $CD11b^+$ monocytes showed reduced spontaneous and SDF-1–mediated migration compared with WT $CD11b^+$ cells (Fig. 2 D). Similarly, CD45KO $CD11b^+$ cells demonstrated reduced homing to the BM of the recipient mice (Fig. 2 E). Live cell images show that immature WT c-$Kit^+$ cells responded to SDF-1 chemotactic signals by cell spreading and the formation of elongated protrusions (Fig. 2 F, left). In contrast, immature CD45KO c-$Kit^+$ cells remained mostly round, forming only short cell protrusions in response to SDF-1 (Fig. 2 F, right). In vivo homing assays demonstrated the inferior homing of CD45KO c-$Kit^+$ progenitors to the BM and spleen, in comparison to their WT counterparts (Fig. 2 G). Interestingly, CD45KO spleen-derived colony-forming progenitor cells also exhibited poor homing potential to the BM and spleen of recipient mice (Fig. 2 H). Additionally, in a functional repopulation assay, CD45KO spleen-derived cells showed a reduced potential to engraft the BM of WT recipients, also showing defects in primitive repopulating cells (Fig. 2 I). These results demonstrate systemic cell autonomous defects in CD45KO cell motility.

### Reduced MMP-9 secretion and hyperadhesion of CD45KO cells

To elucidate possible mechanisms underlying CD45-regulated cell motility, we assessed the secretion potential of MMPs, in particular of MMP-9, which is involved in hematopoietic cell invasion and is up-regulated upon stress signals (4, 9, 26). BM and PB MNCs of CD45KO mice secreted lower levels of pro–MMP-9 compared with their WT counterparts (Fig. 3, A and B). In vivo 3-d G-CSF stimulations increased secretion of this enzyme by both WT BM and PB MNCs (Fig. 3, A and B). In contrast, MNCs obtained from G-CSF–treated CD45KO mice still secreted significantly lower levels of pro–MMP-9 (Fig. 3, A and B).

Retention of leukocytes in the BM requires a concomitant balance of adhesion and detachment. The role of CD45 in these processes was therefore studied. We found significantly elevated expression levels of activated β1 integrin in BM MNCs obtained from CD45KO mice (twofold higher than their WT counterparts; Fig. 3 C). This phenomenon was associated with an increased adhesion capacity to FN (Fig. 3 D). This hyperadhesion of CD45KO cells may further explain their poor motility both in vitro and in vivo.

### CD45 deficiency leads to hyperactivation of the Src signaling pathway

Several papers have demonstrated the importance of Src kinases, the natural substrate of CD45, in integrin-mediated adhesion in various mature lymphoid and myeloid cells (27, 28). We thus examined the Src phosphorylation status and activity during steady state and in response to G-CSF administration. G-CSF stimulations of WT mice led to a reduction in Src phosphorylation and activity in BM MNCs (Fig. 3, E and F). Notably, these modulations in Src were inversely correlated with CD45 expression (Fig. 1, A and B). Interestingly, MNCs derived from the BM of untreated CD45KO mice displayed enhanced Src phosphorylation and activity (Fig. 3, E and F), and G-CSF stimulations only slightly reduced it in these CD45KO cells. Src family kinases were shown to negatively regulate the mitogen-activated protein kinase cascades, particularly extracellular signal-regulated kinase (Erk) activation (29). As Fig. 3 G shows, G-CSF treatment activated Erk protein in WT-derived BM cells, suggesting that Src kinase activity is indeed reduced. Interestingly, in the CD45KO BM, where Src kinases are hyperactive, Erk proteins are inhibited, as demonstrated by the low phosphorylation of Erk both in untreated and in G-CSF–treated mice. Finally, inhibition of Src proteins in CD45KO BM-derived cells using the PP2 inhibitor, which down-regulates the hyperactivity of Src proteins, increased migration of these CD45KO cells to a gradient of SDF-1 (Fig. 3 H). These results ultimately demonstrate the link between CD45, Src kinase activity, and the regulation of motility properties.

### Impaired receptor activator of NF-κB ligand (RANKL)–induced progenitor mobilization in CD45KO mice

Next, we chose to specifically stimulate CD45KO mice in vivo by injecting RANKL, which was shown to activate osteoclasts leading to preferential expansion and mobilization of immature cells (16). RANKL stimulation in WT mice increased the

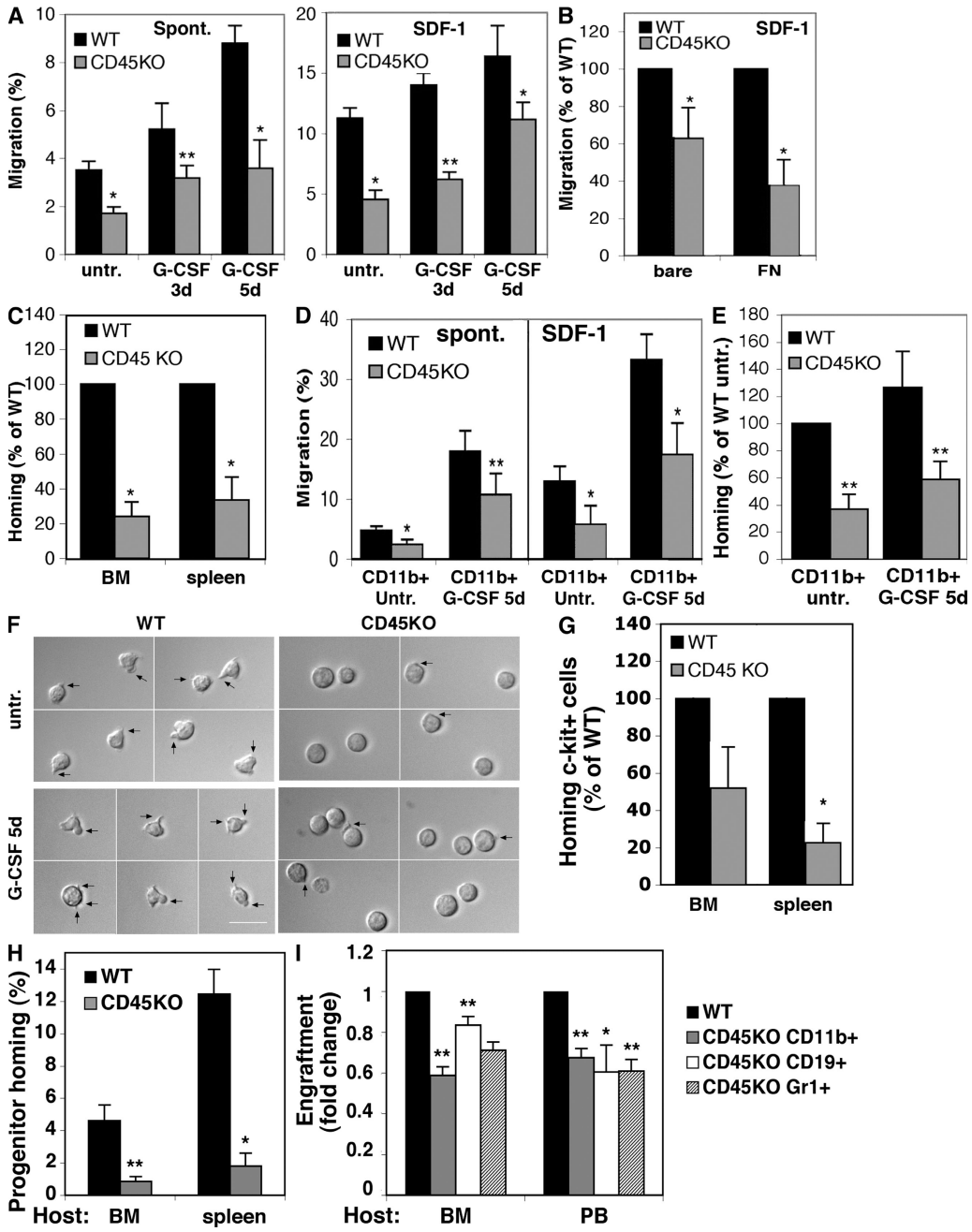


**Figure 2. Impaired migration and reduced response to SDF-1 by CD45KO progenitors.** (A and B) In vitro migration of MNCs from the BM of CD45KO or WT mice either untreated or treated with G-CSF for 3 or 5 d. Cells were allowed to migrate without (spont.) or with addition of SDF-1 to the lower well. (B) Migration of WT and CD45KO BM MNCs of untreated mice through bare or FN-coated filters toward SDF-1. (C) Homing of BM MNCs derived from untreated WT and CD45KO mice to the BM and spleens of recipient NOD/SCID mice 3 h after transplantation. (D and E). In vitro migration (D) or homing assay (E) of BM CD11b$^+$ cells sorted from the BM of untreated or G-CSF–treated WT or CD45KO mice. (F) c-Kit$^+$ cells were sorted from the BM of WT or CD45KO mice, untreated or treated with G-CSF for 5 d and stimulated in vitro with SDF-1. Representative images demonstrate cell polarization (indicated by black arrows). Bar, 20 µm. (G) Homing of c-Kit$^+$ cells sorted from the BM of WT or CD45KO mice to the BM of NOD/SCID recipient mice 3 h after transplantation. (H) Homing of spleen progenitor cells isolated from WT or CD45KO mice to the BM and spleens of lethally irradiated NOD/SCID/β2 recipients. (I) Percentages of engraftment in WT-recipient BM and PB transplanted with spleen-derived cells from WT and CD45KO mice. Data represent the levels of specific lineages, as indicated. Shown are the means of four recipients in each group ± SE. *, $P < 0.01$; **, $P < 0.05$.

development of tartrate-resistant acid phosphatase–positive (TRAP$^+$) osteoclasts along the endosteum of the trabecular bone, as previously shown (16). However, no increase in TRAP$^+$ osteoclasts was observed in the CD45KO bones (unpublished data). We next tested progenitor cell levels in response to RANKL stimulations for 3 and 5 d. Immature WT progenitors and primitive SKL cells (Fig. 4, A and B, respectively) were expanded in the BM in response to RANKL stimulation, which was contrary to CD45KO cells. Levels of progenitors in the periphery of WT mice, such as the spleen (Fig. 4 C) or PB (Fig. 4 D), were increased, indicating progenitor mobilization. In contrast, CD45KO progenitors were not mobilized by RANKL stimulation for 3 d, and only at moderate levels after 5 d. Next, deeper investigations concerning the degradation of niche components were taken. We found only minor accumulation of soluble SCF in the PB of CD45KO mice in contrast to their WT counterparts (Fig. 4 E). Close examination of the trabecular endosteum, enriched with stem cell niches, demonstrated that in comparison to the WT BM, the niche component osteopontin was poorly degraded in CD45KO bone-lining osteoblasts after RANKL administration for both 3 and 5 d (Fig. 4 F). A broader examination of the entire BM showed a clear osteopontin-degraded product in the fluids of the WT BM after both 3 and 5 d of RANKL treatment (Fig. 4 G). However, degradation products were below the detection levels in CD45KO BM fluids, suggesting impaired osteopontin degradation (Fig. 4 G). These results indicate possible defects in CD45KO osteoclasts, resulting in their impaired response to RANKL and poor release of immature cells from the BM.

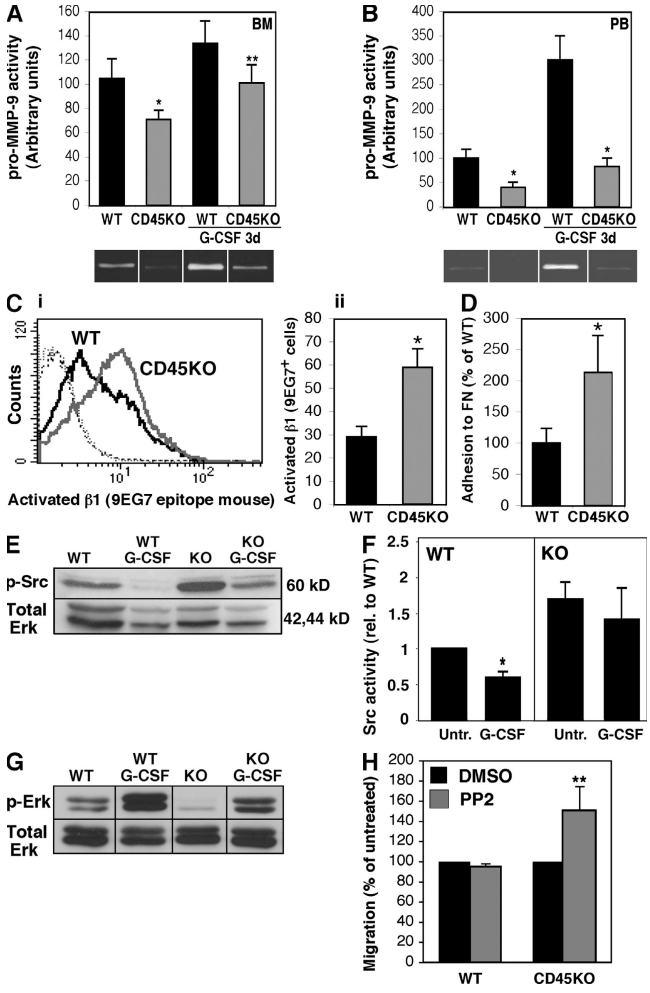


**Figure 3. CD45 deficiency reduces MMP-9 levels and increases cell adhesion via activation of Src kinase.** (A and B) BM or PB MNCs were isolated from CD45KO or WT mice, either untreated or treated with G-CSF for 3 d. Cells were cultured and the activity of MMP-9 in the conditioned media was detected by the gelatin zymography assay. A summary of three independent experiments and representative gel images of BM cells (A) and PB cells (B) is shown (±SD). (C) FACS analyses of the β1-activated epitope 9EG7 in untreated WT or CD45KO BM MNCs. (C, i) Representative histogram of background staining and 9EG7 expression in WT (black line) and CD45KO (gray line). (C, ii) Summary of five independent experiments (±SD). (D) Adhesion assay of WT and CD45KO BM MNCs to FN-coated wells. Shown is a summary of four independent experiments (mean ± SD). (E and F) Western blot analysis of Src phosphorylation or Src activity levels (F) in whole-cell lysates that were prepared from BM MNCs of WT or CD45KO mice, either untreated or after G-CSF injections. Histogram represents a summary of four independent experiments. Values represent the fold change of the control. (G) Western blot analysis for Erk phosphorylation. Lysates were prepared as described in E. (H) SDF-1–induced migration of WT and CD45KO BM MNCs pretreated with 1 μM of the Src inhibitor PP2 or DMSO as a control. Data represent mean ± SD values of three independent experiments and are shown as the fold increase from DMSO-treated cells. *, $P < 0.01$; **, $P < 0.05$.

## Abnormal development and maturation of CD45KO osteoclasts

We continued by investigating the involvement of CD45 in osteoclast development and function. First, we confirmed that mature multinucleated osteoclasts derived from the BM of WT mice express CD45 (Fig. 5 A, top left), whereas, as expected, CD45KO osteoclasts did not express this molecule (Fig. 5 A, bottom left). Next, we observed that CD45KO osteoclasts cultured and developed in vitro demonstrated abnormal morphology (Fig. 5 B). Appearance of the phosphatase TRAP indicates the maturation status and functional stage of bone-resorbing osteoclasts. TRAP staining of CD45KO osteoclasts grown in vitro showed their inability to acquire the flattened, spread morphology and assemble the typical sealing zone that can be seen as a purple ring in the perimeter of WT osteoclasts. In addition, these CD45KO osteoclasts appeared smaller, with a reduced ability to form multinucleated cells. Transcriptional assessment of DC-STAMP mRNA expression revealed that CD45KO BM cells exhibited reduced expression of this receptor (Fig. 5, C and D), which may lead to defects in cell fusion and maturation. We tested additional factors involved in osteoclast development and function, and examined expression of MMP-9 and MT1-MMP expressed by CD45KO osteoclasts. Notably, these cells secreted lower amounts of MMP-9 compared with their WT counterparts (Fig. 5 E), implying reduced osteoclast motility and activity. Moreover, G-CSF, which was shown to activate osteoclast development (30), induced up-regulation of MT1-MMP in WT osteoclasts, whereas expression of this enzyme in CD45KO osteoclasts

remained low, as in the steady state (Fig. 5 F). CD45 deficiency is associated with hyperphosphorylation and activation of its substrate, Src, leading to impaired cell movement (Fig. 3). We therefore assessed osteoclast development in the presence of the Src inhibitor PP2. Src inhibition impaired the development and organization of WT osteoclasts (Fig. 5 G, top), resembling the $Src^{-/-}$ phenotype (31). Conversely, PP2 treatment restored the normal morphology and sealing zone assembly of CD45KO osteoclasts (Fig. 5 G, bottom). Src activity assay confirmed that treating CD45KO osteoclast precursors with PP2 reduced their hyperactive Src to levels equivalent to WT cells (Fig. 5 H), enabling the formation of CD45KO osteoclasts exhibiting a normal phenotype. These results suggest that the expression and function of CD45 and its downstream target Src in monocyte-derived osteoclasts are required for the regulation of normal osteoclast development.

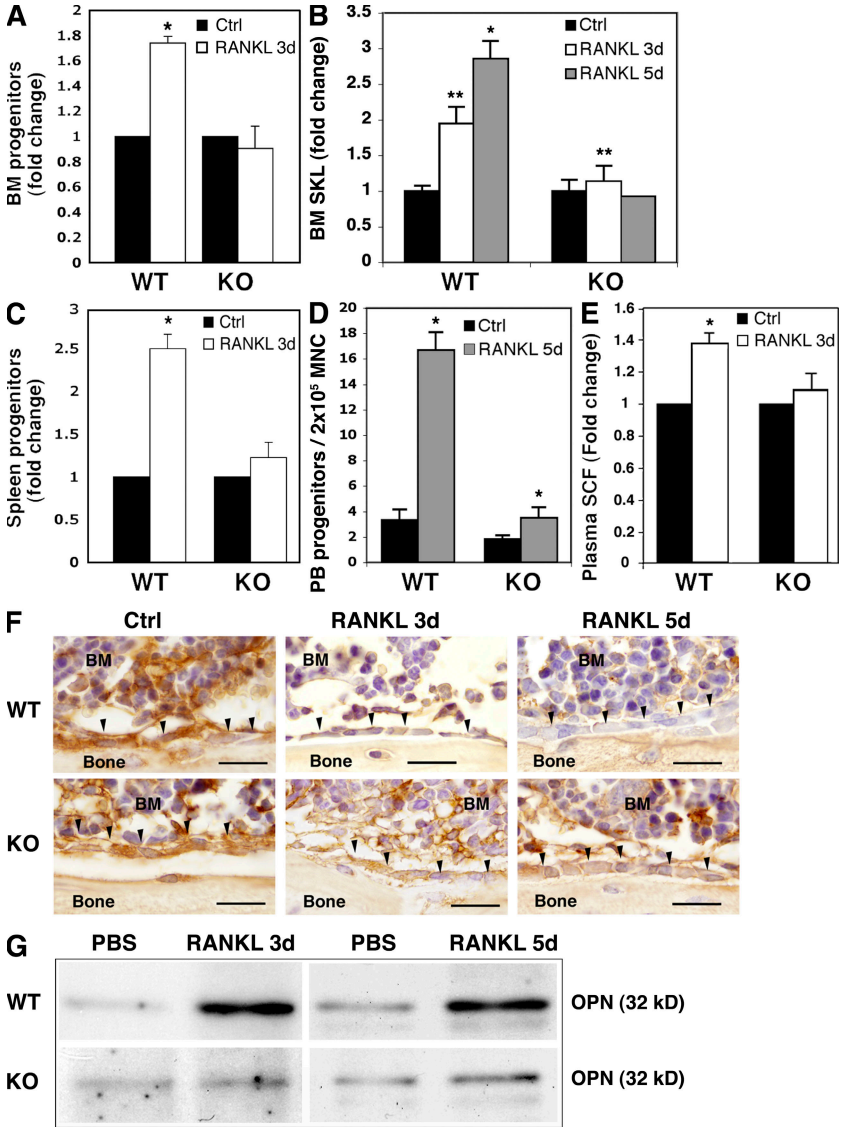


**Figure 4. CD45KO mice show impaired progenitor mobilization and endosteal modulation induced by RANKL.** (A) Colony-forming progenitor cells in the BM of WT and CD45KO mice after RANKL treatment for 3 d. Values indicate fold changes compared with control mice ± SE (*, $P < 0.01$). (B) The percentage of SKL primitive cells in the BM of WT versus CD45KO mice after treatment with RANKL for 3 or 5 d. Values indicate the fold changes compared with control mice ± SE (*, $P < 0.02$; **, $P < 0.05$). (C) Colony-forming progenitor cells in the spleens of WT and CD45KO mice after RANKL treatment. Values indicate fold changes compared with control mice ± SE (*, $P < 0.01$). (D) Numbers of colony-forming progenitor cells in the PB of WT and CD45KO mice after RANKL treatment for 5 d (±SE). (E) Soluble SCF levels in the plasma of WT and CD45KO, control, or RANKL-treated mice. Values indicate the fold change in plasma SCF compared with control mice ± SE (*, $P < 0.05$). (F) Immunoreactivity (brown) of osteopontin in femoral metaphyseal trabecules of WT and CD45KO, control, and RANKL-stimulated mice for 3 and 5 d. Black arrowheads indicate endosteal bone-lining osteoblasts. Bars, 20 µm. (G) Western blot analysis of an osteopontin-degraded product (32 kD) in BM superannuates of WT and CD45KO mice after RANKL treatments for 3 and 5 d.

### Abnormal bone microenvironment and defective hematopoiesis caused by reduced osteoclast function in CD45KO mice

The reduced response of CD45KO mice to RANKL stimulations further suggested a defective function of CD45KO osteoclasts after their activation. Accumulation of pyridinoline (PYD) in the mouse plasma reflects an ongoing bone resorption process as a result of osteoclast function. We found lower levels of PYD in the plasma of CD45KO mice, indicating impaired osteoclast resorbing activity (Fig. 6 A). In addition, we tested the levels of plasma osteocalcin as a marker for bone turnover. CD45KO mice demonstrated reduced amounts of osteocalcin in the plasma in comparison to their WT controls (Fig. 6 B). Hence, these findings suggested that bone-remodeling processes are impaired in CD45KO mice, resembling mild osteopetrosis. A three-dimensional μCT scanning

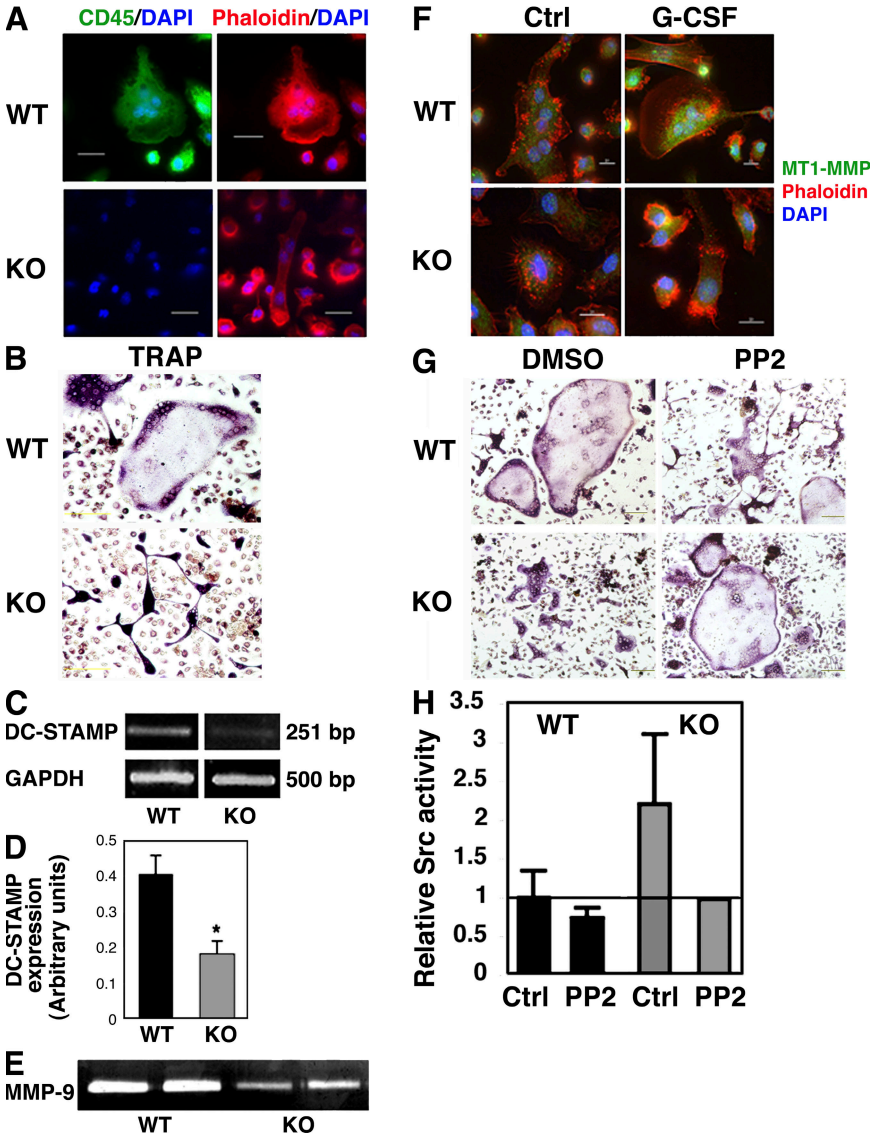


**Figure 5. Defective maturation of CD45KO osteoclasts in vitro involving impaired expression of MMPs, DC-STAMP, and Src kinase.** (A) BM-derived osteoclasts from WT (top) and CD45KO (bottom) mice immunolabeled for CD45 expression (green), and stained for polymerized actin (red) and nuclear DNA (blue). Bars, 20 μm. (B) TRAP staining (purple) of BM-derived WT (top) and CD45KO (bottom) osteoclasts. Bars, 200 μm. (C and D) Semiquantitative PCR analysis for DC-STAMP mRNA levels in WT and CD45KO BM-derived cells. (C) Representative PCR image. (D) Summary of four independent experiments showing the ratio between DC-STAMP and GAPDH mRNA expression (±SE; *, $P < 0.01$). (E) Conditioned medium of WT versus CD45KO BM-derived osteoclasts was tested for the activity of secreted MMP-9 in a gelatin zymography assay. (F) WT and CD45KO BM-derived osteoclasts cultured with or without G-CSF were immunolabeled for expression of MT1-MMP (green), and stained for polymerized actin (red) and nuclear DNA (blue). Bar, 10 μm. (G) TRAP staining (purple) of BM-derived WT (top) and CD45KO (bottom) osteoclasts cultured in vitro in the presence of DMSO vehicle (left) or the Src inhibitor PP2 (right). Bars, 200 μm. (H) Src activity assay for osteoclast precursors incubated with 1 μM PP2 or DMSO (ctrl) for 5 d. Values indicate the fold changes of WT control mice ± SE (indicated by a horizontal line), showing a representative experiment.

of WT and CD45KO mice femurs was applied to analyze the trabecular and cortical microarchitecture. Based on a previous paper showing preferred localization of stem cells close to the bone edge (32), two regions of interest were determined: the first included 2 mm from the distal metaphysis (region 1), and the second was 1 mm ahead toward the diaphysis (region 2). Various bone morphometric and steorologic parameters, including bone volume and bone mineral mass; trabecular volume, trabecular number (Tb.N), and trabecular thickness; and the gaps between the trabecules were measured. The most prominent difference was the distribution of femoral trabecules. In WT mice, most of the femoral trabecules were found near the growing plates of the bone edge, in region 1 (Fig. 6 C, red frame). However, an abnormal pattern of trabecular distribution was observed in the femurs of CD45KO mice, demonstrating a substantially higher number of trabecules in region 2 (Fig. 6 C, yellow frame). Accordingly, stereological analyses of CD45KO bones showed lower Tb.Ns at region 1 (red frame, 75 ± 1.5%) and higher numbers at region 2 (yellow frame, 122 ± 11%) compared with the femurs of WT mice. Interestingly, in vivo TRAP staining of bone sections demonstrated higher numbers of CD45KO TRAP$^+$ cells along the trabecular endosteum, in comparison to their WT counterparts (Fig. 6 D). Similarly, a significantly larger portion of the CD45KO bone surface was covered with TRAP$^+$ cells (Fig. 6 E), apparently compensating for their impaired function, as previously suggested in other osteoclast-defective models (18, 33). Of note, previous studies showed that osteopetrosis

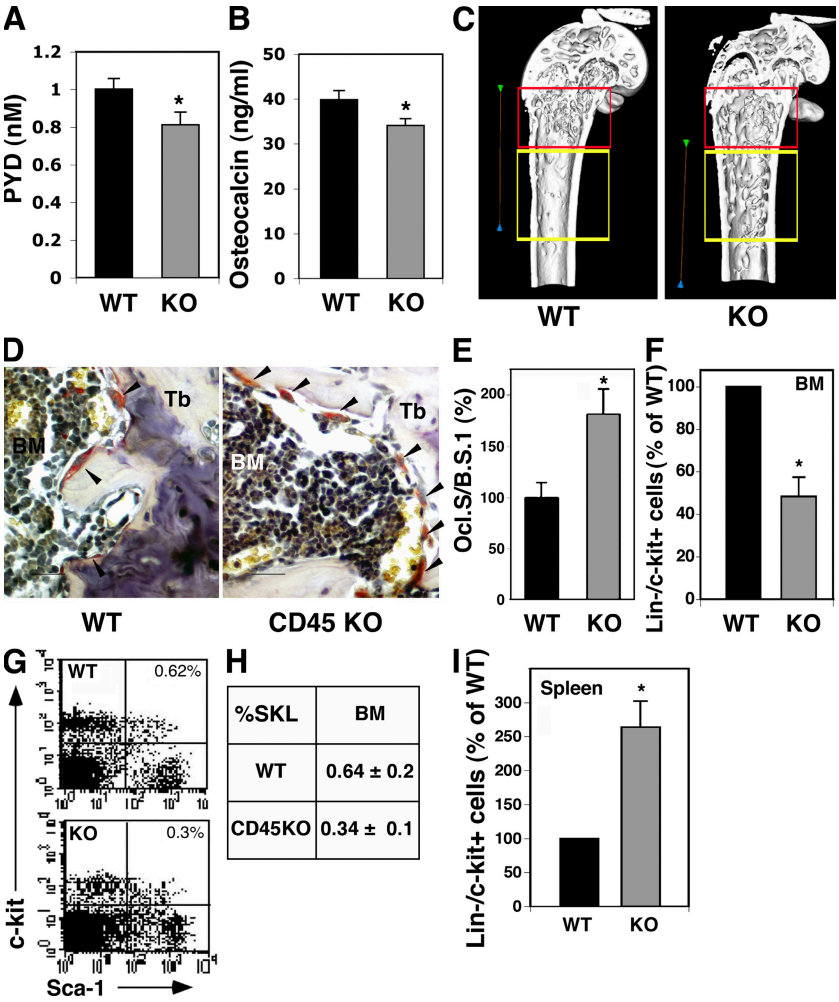


**Figure 6. Reduced osteoclast function in CD45KO mice is associated with elongated trabecular zone and irregular localization of progenitors.** (A) Plasma levels of PYD indicating bone resorption in WT and CD45KO. (B) Plasma levels of osteocalcin in WT and CD45KO mice. Values represent the mean ± SE (*, $P < 0.05$). (C) Three-dimensional constructions of the distal femurs of WT and CD45KO mice. The red frame indicates the metaphyseal region, near the bone growing plates, and the yellow frame indicates a region 1 mm ahead toward the diaphysis (see Materials and methods). Bars, 2 mm. (D) TRAP staining of femoral bone sections. Osteoclasts stained in red (arrowheads) are shown along the metaphyseal trabecules (Tb). (E) The ratio between osteoclast surface and bone surface (Ocl.S/B.S). Data are presented as the percentage of WT cells ± SE (*, $P < 0.05$). (F–H) Flow cytometry analyses of BM immature Lin$^-$/c-Kit$^+$ progenitors (F), presented as the percentage of WT (mean ± SE), and the more primitive SKL stem cells. A representative FACS plot (G) and summary (H) indicate lower levels of these primitive cells in the BM of CD45KO mice. *, $P < 0.01$. (I) Flow cytometry analyses of spleen-derived immature Lin$^-$/c-Kit$^+$ progenitors, presented as the percentage of WT (mean ± SE). Numbers indicate higher levels of these primitive cells in the spleen of CD45KO mice, *, $P < 0.01$.

and other defects associated with changes in the architecture of the bone are accompanied by alterations in the hematopoietic stem cell pool size and location (33, 34). We therefore anticipated that the abnormal bone microenvironment in CD45KO mice is related to altered hematopoietic stem and progenitor cell retention. Despite the regular cellularity of mature BM leukocytes and normal differential counts of circulating mature cells (Fig. 1 E), we identified lower numbers of immature $Lin^-/c\text{-}Kit^+$ cells (Fig. 6 F) and the primitive SKL subset (Fig. 6, G and H) in the BM of CD45KO mice. Notably, significantly higher numbers of these undifferentiated cell populations were documented in the spleens of CD45KO mice in comparison to their WT counterparts (Fig. 6 I). Yet, despite their increased levels, CD45KO spleen-derived progenitors showed inferior homing and repopulation potentials (Fig. 2 I).

### Mutual defects in the CD45KO BM environment and hematopoietic cells in response to rapid mobilization

Our results suggested that both environmental and cell-intrinsic defects can account for the impaired progenitor mobilization in CD45KO mice. To directly dissect these options, we established two sets of chimera models in which CD45KO mice were tested either as recipients or donors compared with WT mice. In the first set of experiments, WT and CD45KO mice were used as recipients for WT donor cells. In this setting, we observed lower engraftment levels of WT donor cells in CD45KO recipients compared with WT recipients (Fig. 7 A). This suggested an impaired ability of the CD45KO BM environment to support stem cell maintenance. Next, we studied rapid mobilization by injecting the CXCR4 antagonist AMD3100, which was shown to induce mobilization without mediating cell expansion in the BM. Our results showed that after AMD3100 administration, WT (normal) donor cells have impaired mobilization in CD45KO compared with WT hosts (Fig. 7 B). These findings demonstrated that the CD45KO BM environment failed to facilitate normal mobilization. In the second set of experiments, high cell doses of WT and CD45KO cells were used as donor cells to repopulate WT recipients. In this set the mobilization potential of CD45KO cells in a normal environment was further assessed. In highly engrafted mice, AMD3100 stimulation resulted in only a minor cell mobilization when CD45KO cells served as donors, compared with their WT counterparts, although their BM environment was normal (Fig. 7 C). These experiments suggested that CD45 deficiency results in multiple defects, combining both cell autonomous and environmental mechanisms.

## DISCUSSION

In this study, we identified important roles for the panleukocyte CD45 in key processes of immature hematopoietic cell function: its BM retention and release to the periphery, processes that are dramatically affected by stress conditions. By using the CD45KO mouse model, we investigated two major parameters involved in progenitor motility and location, including intrinsic properties and environmental regulation. First, we revealed autonomous defects in CD45KO cell motility into and out of the BM compartment, including reduced mobilization and homing of mature leukocytes and immature progenitor cell populations derived from different organs. We suggest that CD45 regulates two cellular processes that have key roles in the migration and retention of leukocytes in general,

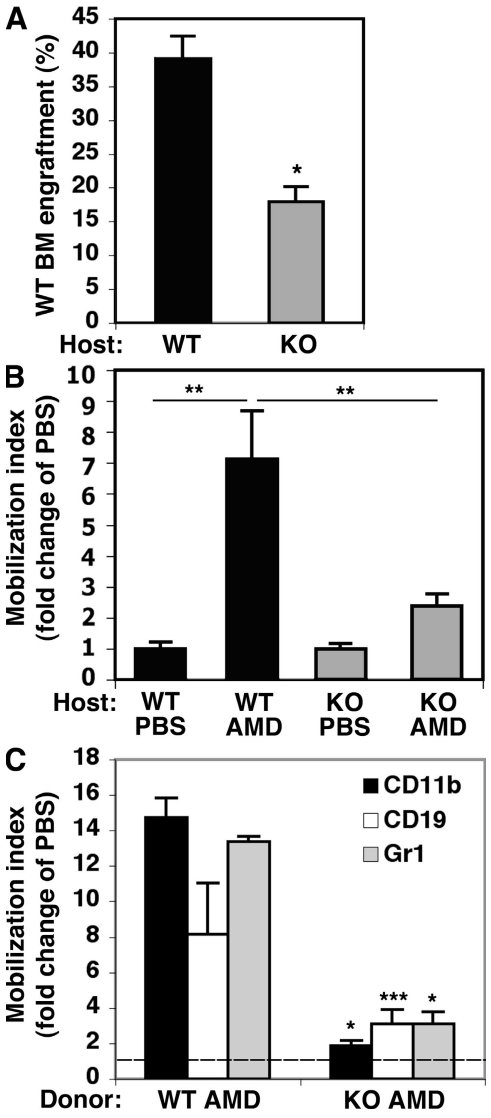


**Figure 7. Defective engraftment and reduced rapid mobilization in CD45KO chimeras.** (A) Percentage of donor-derived WT cells in the BM of WT and CD45KO recipients. Shown is a summary of seven mice in each group (±SE; *, $P < 0.01$). Values demonstrate reduced engraftment levels in CD45KO hosts. (B) AMD3100-induced mobilization of donor WBCs in the PB of WT and CD45KO hosts. Values indicate fold change of mobilization index compared with PBS control mice (±SE). **, $P < 0.05$. (C) Rapid mobilization of WT and CD45KO donor cells. WT chimeric hosts were injected with PBS or AMD3100 and were tested for the presence of donor-derived cells in the PB. The mobilization index of specific lineages was tested, as indicated in the figure legend. Values indicate the fold change compared with PBS control mice, which are marked as a dashed line (mean ± SE). *, $P < 0.01$; ***, $P = 0.07$.

and progenitors in particular: proteolytic enzyme secretion and adhesion interactions. Lower secretion of MMP-9 by CD45KO BM MNCs after G-CSF stimulation implies that CD45 regulates MMP activation, and may thus further explain the reduced egress of CD45KO leukocytes. Corroborating our findings, mouse multiple myeloma CD45KO cells also secrete lower levels of MMP-9, correlating with their reduced invasive capacities compared with $CD45^+$ cells (35).

BM-derived cells lacking CD45 have increased activation of β1 integrins and hyperinduction of adhesion properties, demonstrating that CD45 is a negative regulator of signaling cascades, inducing cell detachment and release. We found that Src kinase, the CD45 substrate, is a potential target by which CD45 regulates the migration of hematopoietic cells. Indeed, Src kinase inhibition enhanced CD45KO cell motility, demonstrating that Src activity is unbalanced in these cells. Several studies support the involvement of Src kinases in adhesion and motility properties. Src kinases were shown to regulate β1 and β2 integrins in different cells and cell lines (28, 36). Moreover, in mice deficient in members of the Src family, immature, hematopoietic $Sca\text{-}1^+$ cells demonstrated increased homing (37), and primitive, BM-derived SKL cells showed enhanced G-CSF–induced mobilization that was associated with elevated MMP-9 and accelerated breakdown of vascular cell adhesion molecule 1 (38). In line with these studies, our results demonstrate the opposite effects when Src is hyperactive because of CD45 deficiency. Still, such fundamental defects in the motility of both CD45KO progenitors and maturing leukocytes strongly suggest that additional pathways are also imbalanced by the lack of CD45 function. This is especially apparent in the defective cell polarization in response to chemotactic signals of CD45KO $c\text{-}Kit^+$ progenitors. Moreover, SDF-1 is considered as a survival factor for stem and progenitor cells (39). Thus, the impaired ability of immature CD45KO $c\text{-}Kit^+$ cells to normally respond to SDF-1 stimulation may further explain their inferior retention in the BM.

Previously, we suggested that interactions between hematopoietic stem and progenitor cells with their BM microenvironment are mutual (5, 11). We further reveal that CD45 also plays a role in progenitor mobilization by regulating components of the BM microenvironment. Reduced progenitor expansion and release in response to RANKL activation in CD45KO mice was associated with impaired modulation of the stem cell niche regulating components osteopontin and SCF. Osteopontin was shown to negatively regulate and limit the number of endosteal stem cells (40, 41). The impaired degradation of osteopontin in the endosteum of RANKL-treated CD45KO mice may explain the low numbers and reduced expansion of progenitors and stem cells in their BM. In addition, it was previously shown that shedding of membrane-bound SCF by MMP-9 shifts stem cells from a quiescent to a proliferative state, enabling their release from the BM (9). The impaired resorption activity and the low secretion of MMP-9 by CD45KO osteoclasts may also contribute to the reduced progenitor expansion in the CD45KO BM, a prerequisite step for immature cell mobilization.

Osteoclasts derived from hematopoietic precursors in the BM of CD45KO mice show abnormal morphology and function both in vitro and in vivo, reflecting mild osteopetrosis. Of note, osteoclasts derived from precursors in the spleen exhibited the same defective phenotype (unpublished data), although the numbers of hematopoietic progenitors were higher in the CD45KO spleens. This demonstrates that the decreased osteoclast numbers are not caused by the lack of progenitor cells but rather an intrinsic defect in osteoclast differentiation. Our investigations further showed that CD45 regulates osteoclast formation via controlling Src kinase activity and DC-STAMP expression. In support of our findings, previous reports showed that osteoclasts derived from $DC\text{-}STAMP^{-/-}$ mice were $TRAP^+$ MNCs exhibiting a reduced bone-resorbing activity (17). Interestingly, $DC\text{-}STAMP^{-/-}$ osteoclasts demonstrated enhanced Src expression, suggesting a link between these two regulators (17). Thus, our data propose a role for the CD45–Src axis in osteoclast fusion and maturation. In addition, low expression of MMPs in CD45KO osteoclasts showed that by regulating MMP-9 and MT1-MMP expression, CD45 is eventually involved in osteoclast motility and bone degradation activity (42, 43). These defects in osteoclasts may thus explain the poor mobilization observed in CD45KO mice. However, distinguishing between the environmental versus hematopoietic effects using chimera models revealed a parallel and perhaps additive impact of both compartments on progenitor retention and mobilization potentials.

The abnormal phenotype and activity of CD45KO osteoclasts are associated with lower numbers of trabecules in the femoral metaphysis, a region known to harbor stem cells (32). Mouse models of severe osteopetrosis exhibit extramedular hematopoiesis, demonstrating lower levels of stem and progenitors cells in the BM caused by several bone structure defects, and higher levels of progenitor cells in the spleen (33, 44). CD45KO mice demonstrated a similar phenotype of the primitive SKL pool size and location driven by multiple defects of both the CD45KO primitive cells and their osteoclast progeny. The reduction in CD45KO primitive cells in the BM is complementary to previous findings showing that $Lyn^{-/-}$ mice (members of the Src kinase family) display higher numbers of primitive SKL cells in the BM (45), demonstrating the central role of the CD45–Src cascade in stem cell retention. Our findings indicate that stem and progenitor cells can modulate their CD45 expression and signaling via Src kinase, influencing their retention, survival, and motility. Moreover, CD45KO spleen progenitors, which are not directly influenced by osteoclasts, exhibited poor mobility and repopulation potentials, and an unusual distribution of these progenitors was observed between the spleen and the PB. However, previous studies showed that in normal settings, spleen progenitors reside in equilibrium with the blood, suggesting no barrier between these organs (46), as opposed to the BM (6, 46). Hence, progenitor accumulation in the spleen may also be affected by the impaired intrinsic ability of CD45KO spleen progenitors to traffic to the circulation. Additional factors may also be involved, including increased survival and/or proliferation of these progenitor cells in extramedullary locations such as the spleen.

Our results suggest that hematopoietic stem cells and their leukocyte progeny have dual CD45-mediated self-regulation modes: their motility, proliferation, and adhesion are autonomously and dynamically regulated. In addition to stem cell regulation by the niche, functional CD45 is needed for osteoclast development and activity, which indirectly affect hematopoiesis and the progenitor pool size via interactions with the bone and BM stromal cells. This notion of a dynamic cross talk between all components of the system is also supported by a recent study, which shows that primitive signaling lymphocyte activation molecule stem and progenitor cells can directly regulate osteoblast development (47). Collectively, our results reveal that hematopoietic stem and progenitor cells are involved in regulating their own levels and the dynamic BM microenvironment via their osteoclast progeny, which require modulated CD45 activity.

## MATERIALS AND METHODS

**Mice.** All experiments were approved by the animal care committee of the Weizmann Institute. The experiments were performed on CD45 exon 6–deficient mice (provided by T. Mak, University of Toronto, Toronto, Canada), which were bred and maintained under defined flora conditions at the Weizmann Institute. Age- and sex-matched C57BL/6 (CD45.2) mice (Harlan) were used as a WT control. All mice used were 6–8 wk of age at the onset of the experiments.

**Stress-induced mobilization.** Mice received a daily s.c. injection of 300 μg/kg G-CSF (Filgrastim; Roche) for 3 or 5 consecutive days and were killed 4–6 h after the last injection. Single injections of 12.5 mg/kg LPS (*Escherichia coli* serotype O111:B4; Sigma-Aldrich) were administrated i.p. Mice were killed 16 h after injection. 2 μg of mouse RANKL (R&D Systems) was injected into 5–6-wk-old WT and CD45KO mice, s.c. over the femur, twice a day for the first 3 d followed by 2 d of rest, or for 5 consecutive days.

**Homing assay.** $5 \times 10^6$ mouse BM MNCs per mouse, or $2.5 \times 10^6$ $CD11b^+$ or $c\text{-}Kit^+$ sorted cells per mouse, were prelabeled with CFSE dye (5 μM/$10^7$ cells; Invitrogen) and i.v. injected into NOD/SCID mice. Recipient mice were killed after 3 h, and the number of $CFSE^+$ cells that reached the BM and spleens of recipient mice was determined by FACS. The homing of progenitor cells was examined as previously described (48) and modified using spleen cells by injecting $20 \times 10^6$ total spleen cells into lethally irradiated (600 cGy from a cesium source) NOD/SCID/$\beta2^{-/-}$ mice. A fraction of the injected cells was plated in colony assays to quantify the number of injected CFU-Cs. Recipients were killed 18 h after injections, and fractions of BM and spleen ($1–2 \times 10^6$ cells) were plated in methylcellulose medium to find the numbers of functional CFU-Cs (progenitors) that lodged to these organs. Homing efficiency was calculated as the percentage of homed progenitors out of the number of injected CFU-Cs in total spleen or four bones.

**Repopulation and rapid mobilization in chimera models.** Recipient C57BL/6 (CD45.2) or CD45KO (CD45.2) mice were irradiated (600 cGy from a cesium source) and injected 4 h later with $10^6$ total BM cells derived from B6.SJL donors (CD45.1). Alternatively, C57BL/6 recipients were transplanted with $1–10 \times 10^6$ CD45KO BM or $10^6$ spleen-derived cells from B6.SJL or CD45KO mice. PBS (as a control) or 5 mg/kg AMD3100 (Sigma-Aldrich) was injected s.c into chimeric mice 5 wk after transplantation. Engraftment levels and mobilization of donor WBCs in the PB were evaluated 1 h after AMD3100 injections using different combinations of cell staining and were analyzed by FACS. B6.SJL cells in different hosts were detected by tracing $CD45.1^+$ cells, followed by staining with anti–CD45.1-PE/CD45.2-FITC (eBioscience). Detection of CD45KO cells in C57BL/6 hosts was performed by staining with $Lineage^+$/CD45.2 antibodies (eBioscience), evaluating donor cells as $CD19^+$, $CD11b^+$, and $Gr1^+$, which are $CD45^-$ cells. Mobilization index refers to the ratio between BM engraftment level and the amount of donor-derived cells in the circulation.

**Colony-forming assay.** PB samples were subjected to Ficoll separation. Total BM and spleen cells or PB MNCs were seeded ($1.5 \times 10^4$, $5 \times 10^5$, and $2 \times 10^5$ cells/ml, respectively) in semisolid cultures, as previously described (15). Colonies were scored 7 d later under an inverted microscope (CK2; Olympus), applying morphological criteria.

**Flow cytometry analysis.** Membrane expression of different molecules on mouse BM and PB MNCs was detected by flow cytometry, using one- or two-step staining procedures. CD45 expression was assessed with FITC anti–mouse CD45.2 (BD Biosciences). CD45 expression on lineage-specific populations was determined by double staining using anti–CD45-PE (BD Biosciences) and antibodies for lineage markers (CD4- and CD11b-FITC, and c-Kit–allophycocyanin; eBioscience). The percentage of SKL cells in the BM and PB was tested by staining MNCs, as previously described (16). Activated mouse β1 was detected by using anti-CD29 (clone 9EG7; BD Biosciences) and secondary PE–donkey anti–rat (Jackson ImmunoResearch Laboratories). After staining, cells were washed and analyzed on a FACSCalibur (Becton Dickinson) using CellQuest software.

**Sorting for $CD11b^+$ and $c\text{-}Kit^+$ cells.** Total BM cells from untreated mice or mice treated with G-CSF for 5 d were stained using anti–CD11b-FITC and anti–c-Kit–APC. Cells were sorted to these two populations simultaneously using a FACSAria (Becton Dickinson). Cells were washed and tested applying in vitro and in vivo assays.

**Migration assay.** Chemotaxis assays were performed in Costar transwells (6.5-mm diameter, 5-μm pore size; Corning). Upper filters were untreated (bare) or precoated overnight with 25 μg/ml FN at 4°C (Millipore). $10^5$ mouse BM MNCs were added to the upper filters and were allowed to migrate toward 50 ng/ml SDF-1α (PeproTech) for 2 h. Migrating cells were counted using a FACSCalibur. CD45KO BM MNCs were pretreated with 1 μM of the Src inhibitor PP2 (EMD), or as a control with the PP2 solvent DMSO for 30 min at 37°C. The cells were then washed and submitted to migration toward 50 ng/ml SDF-1 and analyzed as described.

**Cell polarization microscopy images.** Response to 200 ng/ml SDF-1 of $c\text{-}Kit^+$–sorted cells was observed using a 40× objective (NA = 1.35; Olympus) on uncoated μ slides (Integrated BioDiagnostics). Phase-contrast images were acquired using scientific-grade charge-coupled device (CCD) camera (LIS-700; Applitech) and processed by the DeltaVisionRT system using SoftWoRx software (Applied Precision).

**Adhesion assay.** 96-well plates were coated by overnight incubation with 25 μg/ml FN at 4°C, washed with PBS, and blocked with 0.1% BSA. $2.5 \times 10^5$ WT or CD45KO BM MNCs per well were allowed to adhere to the plates for 16 h at 37°C in serum-free RPMI 1640. Nonadherent cells were washed twice in PBS. Adherent cells were collected in 200 μl PBS buffer plus 0.5 mM EDTA. The number of adherent cells was determined by FACS analysis using a FACSCalibur.

**MMP-9 zymography.** Zymography assay was performed as previously described (4), with the following modifications. BM and PB MNCs were incubated in vitro at 37°C ($10^5$ cells per 100 μl of serum-free RPMI 1640) for 40 h. For measurement of osteoclast-secreted MMP-9, total BM cells were cultured with M-CSF and RANKL, as previously described (16). The resulting conditioned medium was collected and loaded (10 μl) on 10% SDS-PAGE gels containing 1 mg/ml gelatin.

**Immunoblotting.** Whole-cell lysates were prepared from BM MNCs of WT or CD45KO mice, intact or after G-CSF injections for 3–5 d. Lysates were obtained by a 15-min incubation with modified RIPA buffer (20 mM Hepes [pH 7.3], 150 mM NaCl, 10% glycerol, 0.1% SDS, 1% Triton X-100,

2 mM EDTA, 2 mM EGTA, 0.5% deoxycholate, 50 mM βGP, and 50 mM NaF) freshly supplemented with 1% protease inhibitor cocktail (Sigma-Aldrich) and 0.2 mM pervanadate (Sigma-Aldrich). 50 μg of total protein was separated on 10% SDS-PAGE and transferred to nitrocellulose membranes. The membranes were blocked with TBST (5 mM Tris, 154 mM NaCl, 0.1% Tween-20 [pH 7.6]) containing 5% milk and probed with rabbit anti–human/mouse phospho-Src (Invitrogen), rabbit anti–human/mouse ERK1 ($pThr^{202}$/$pTyr^{204}$) and ERK2 ($pThr^{185}$/$pTyr^{187}$; Sigma-Aldrich), or rabbit anti–total ERK1/2 (Sigma-Aldrich), as a control for total protein. Osteopontin expression was evaluated in BM superannuates, separated on 10% SDS-PAGE (20 μg). Polyclonal anti–mouse osteopontin antibodies (R&D Systems) were used to detect the 32-kD degraded product, as previously described (49).

**Src activity assay.** Whole-cell lysates were prepared from BM MNCs and sorted $CD11b^+$ cells. Alternatively, lysates were prepared from osteoclast precursors grown for 5 d in the presence of RANKL and 20 ng/ml M-CSF supplemented with 1 μM PP2 or DMSO vehicle. Lysis was performed using HNTG lysis buffer (20 mM Hepes [pH 7.5], 150 mM NaCl, 1% Triton X-100, 10% glycerol, 1 mM EDTA, 1 mM EGTA, 50 mM NaF) freshly supplemented with 1% protease inhibitor cocktail, 0.2 mM pervanadate, and 0.5 mM okadaic acid (A.G. Scientific). Src kinases were immunoprecipitated by incubating cell lysates with 1 μg of anti–v-Src antibodies (EMD) for 2 h at 4°C. Protein G plus agarose beads (Santa Cruz Biotechnology, Inc.) were added to the mixture and incubated for an additional 12 h at 4°C. Immunocomplexes were precipitated after three washes with HNTG wash buffer (20 mM Hepes [pH 7.5], 150 mM NaCl, 0.1% Triton X-100, 10% glycerol, 1 mM EDTA, 1 mM EGTA, 50 mM βGP, 50 mM NaF, 1 mM sodium orthovanadate) and a final wash with Src kinase buffer (20 mM MOPS, 5 mM $MgCl_2$). Src kinase activity was tested using a tyrosine kinase activity assay kit (Millipore) according to the manufacturer's instructions. Src activity in BM samples was calculated in correlation to the total amount of Src that was precipitated in each sample stated by immunoblot assay.

**μCT imaging and trabecular morphometry.** Femurs from CD45KO and WT control mice were removed, disarticulated from the pelvic bone and tibia, cleaned of soft tissues, and stored at −20°C. After thawing at room temperature, bones were scanned using a μCT device (eXplore Locus SP; General Electric) with custom software (version 5.2.2; MicroView). Scanning was performed with 80-kV x-ray voltage, 80-μA current, 400-ms integration time, and 8-μm pixel size. Based on preliminary work, two volumes of interest (VOI) were defined (Fig. 6 C). The first VOI consisted of the distal metaphyseal region, defined as starting at a distance of 32 image slices (250 μm) from the growth plate in the direction of the diaphysis, and extending a further 220 slices (1.75 mm) in the same direction. The second proximal metaphyseal VOI started from the end of the previous VOI and extended a further 125 slices (1 mm) in the same direction. The trabecular volume was separated from the surrounding cortical shell by manual segmentation, and a direct three-dimensional model (50) was used to evaluate the Tb.N.

**Osteoclast immunocytochemical staining.** Total BM cells were seeded on glass cover-slips ($10^6$ cells/1 ml) and cultured for 6 d in α-MEM supplemented with 20 ng/ml M-CSF (PeproTech) and RANKL that were changed every other day. Where indicated in the figures, culture medium was supplemented with 200 ng/ml G-CSF (Filgrastim; Roche). Samples were fixed with 3% paraformaldehyde (Merck), permeabilized with 0.5% Triton X-100 (Sigma-Aldrich), and immunolabeled at room temperature in a humidified chamber with FITC-conjugated anti-CD45.2 (eBioscience) or rabbit anti–mouse/human MT1-MMP polyclonal antibody (Millipore), followed by secondary goat anti–rabbit–Alexa Fluor 488. TRITC-phalloidin and DAPI (Sigma-Aldrich) were added. Images were acquired using scientific-grade CCD camera and processed by the DeltaVisionRT system using SoftWoRx software.

**TRAP staining of bone sections and osteoclasts.** TRAP staining of bone sections and osteoclasts was performed as previously described (16). For osteoclast formation in vitro, BM cells were seeded in 96-well plates ($10^5$ cells/0.2 ml) and cultured with M-CSF and RANKL, as previously described (16). In some experiments, the culture medium was supplemented with 1 μM of the Src inhibitor PP2 or its vehicle DMSO in the respective concentration.

**Immunohistochemistry of osteopontin and SDF-1.** Bone sections were prepared and stained as previously described (16).

**ELISA for mouse SCF.** Blood plasma samples were obtained from control and RANKL-treated mice and tested for SCF by ELISA, as previously described (16).

**ELISA for PYD and osteocalcin.** We tested plasma PYD (Metra; Quidel Corp.) and osteocalcin (Biomedical Technologies, Inc.) on frozen plasma samples according to the manufacturers' instructions.

**Semiquantitative RT-PCR for DC-STAMP.** We prepared cDNA from mouse BM cells using standard protocols. We performed semiquantitative PCR analysis for DC-STAMP expression for 35 cycles: 95°C for 1 min, 60°C for 1 min, and 72°C for 1 min. We used the following primer sequences: 5′-GGGTCTCAACACCACGAACT-3′ and 5′-GACTCT-GTTTGCCCAGCTTC-3′ (251 bp).

**Statistical analysis.** Significance levels of the data were determined by the Student's *t* test using Microsoft Excel.

The authors would like to thank Prof. Tak Mak for providing the CD45 KO mice; Dr. E. Zelzer for the usage of the μCT machine; and Prof. G. Wagemaker, Prof. A. Globerson, Prof. D. Zipori, Prof. R. Alon, Dr. S. Feigelson, and Prof. S. Berrih-Aknin for critical remarks and fruitful discussions.

This work was partially supported by grants from the Israel Science Foundation (796/04), the European Union FP6 Magselectofection, the Charles and David Wolfson Charitable Trust, and the Helen and Martin Kimmel Institute for Stem Cell Research at the Weizmann Institute of Science.

The authors have no conflicting financial interests.

**Submitted: 10 January 2008**
**Accepted: 14 August 2008**

## REFERENCES

1. Yin, T., and L. Li. 2006. The stem cell niches in bone. *J. Clin. Invest.* 116:1195–1201.
2. Thomas, J., F. Liu, and D.C. Link. 2002. Mechanisms of mobilization of hematopoietic progenitors with granulocyte colony-stimulating factor. *Curr. Opin. Hematol.* 9:183–189.
3. Papayannopoulou, T. 2004. Current mechanistic scenarios in hematopoietic stem/progenitor cell mobilization. *Blood.* 103:1580–1585.
4. Kollet, O., S. Shivtiel, Y.Q. Chen, J. Suriawinata, S.N. Thung, M.D. Dabeva, J. Kahn, A. Spiegel, A. Dar, S. Samira, et al. 2003. HGF, SDF-1, and MMP-9 are involved in stress-induced human CD34+ stem cell recruitment to the liver. *J. Clin. Invest.* 112:160–169.
5. Kollet, O., A. Dar, and T. Lapidot. 2007. The multiple roles of osteoclasts in host defense: bone remodeling and hematopoietic stem cell mobilization. *Annu. Rev. Immunol.* 25:51–69.
6. Wright, D.E., A.J. Wagers, A.P. Gulati, F.L. Johnson, and I.L. Weissman. 2001. Physiological migration of hematopoietic stem and progenitor cells. *Science.* 294:1933–1936.
7. Lapidot, T., A. Dar, and O. Kollet. 2005. How do stem cells find their way home? *Blood.* 106:1901–1910.
8. Lapidot, T., and I. Petit. 2002. Current understanding of stem cell mobilization: the roles of chemokines, proteolytic enzymes, adhesion molecules, cytokines, and stromal cells. *Exp. Hematol.* 30:973–981.
9. Heissig, B., K. Hattori, S. Dias, M. Friedrich, B. Ferris, N.R. Hackett, R.G. Crystal, P. Besmer, D. Lyden, M.A. Moore, et al. 2002. Recruitment of stem and progenitor cells from the bone marrow niche requires mmp-9 mediated release of kit-ligand. *Cell.* 109:625–637.

10. Wright, D.E., E.P. Bowman, A.J. Wagers, E.C. Butcher, and I.L. Weissman. 2002. Hematopoietic stem cells are uniquely selective in their migratory response to chemokines. *J. Exp. Med.* 195:1145–1154.
11. Dar, A., O. Kollet, and T. Lapidot. 2006. Mutual, reciprocal SDF-1/CXCR4 interactions between hematopoietic and bone marrow stromal cells regulate human stem cell migration and development in NOD/SCID chimeric mice. *Exp. Hematol.* 34:967–975.
12. Christopherson, K.W., G. Hangoc, C.R. Mantel, and H.E. Broxmeyer. 2004. Modulation of hematopoietic stem cell homing and engraftment by CD26. *Science.* 305:1000–1003.
13. Janowska-Wieczorek, A., L.A. Marquez, J.M. Nabholtz, M.L. Cabuhat, J. Montano, H. Chang, J. Rozmus, J.A. Russell, D.R. Edwards, and A.R. Turner. 1999. Growth factors and cytokines upregulate gelatinase expression in bone marrow CD34(+) cells and their transmigration through reconstituted basement membrane. *Blood.* 93: 3379–3390.
14. Levesque, J.P., Y. Takamatsu, S.K. Nilsson, D.N. Haylock, and P.J. Simmons. 2001. Vascular cell adhesion molecule-1 (CD106) is cleaved by neutrophil proteases in the bone marrow following hematopoietic progenitor cell mobilization by granulocyte colony-stimulating factor. *Blood.* 98:1289–1297.
15. Petit, I., M. Szyper-Kravitz, A. Nagler, M. Lahav, A. Peled, L. Habler, T. Ponomaryov, R.S. Taichman, F. Arenzana-Seisdedos, N. Fujii, et al. 2002. G-CSF induces stem cell mobilization by decreasing bone marrow SDF-1 and up-regulating CXCR4. *Nat. Immunol.* 3:687–694.
16. Kollet, O., A. Dar, S. Shivtiel, A. Kalinkovich, K. Lapid, Y. Sztainberg, M. Tesio, R.M. Samstein, P. Goichberg, A. Spiegel, et al. 2006. Osteoclasts degrade endosteal components and promote mobilization of hematopoietic progenitor cells. *Nat. Med.* 12:657–664.
17. Yagi, M., T. Miyamoto, Y. Sawatani, K. Iwamoto, N. Hosogane, N. Fujita, K. Morita, K. Ninomiya, T. Suzuki, K. Miyamoto, et al. 2005. DC-STAMP is essential for cell–cell fusion in osteoclasts and foreign body giant cells. *J. Exp. Med.* 202:345–351.
18. Boyce, B.F., T. Yoneda, C. Lowe, P. Soriano, and G.R. Mundy. 1992. Requirement of pp60c-src expression for osteoclasts to form ruffled borders and resorb bone in mice. *J. Clin. Invest.* 90:1622–1627.
19. Page-McCaw, A., A.J. Ewald, and Z. Werb. 2007. Matrix metalloproteinases and the regulation of tissue remodelling. *Nat. Rev. Mol. Cell Biol.* 8:221–233.
20. Hermiston, M.L., Z. Xu, and A. Weiss. 2003. CD45: a critical regulator of signaling thresholds in immune cells. *Annu. Rev. Immunol.* 21: 107–137.
21. Penninger, J.M., J. Irie-Sasaki, T. Sasaki, and A.J. Oliveira-dos-Santos. 2001. CD45: new jobs for an old acquaintance. *Nat. Immunol.* 2:389–396.
22. Hermiston, M.L., A.L. Tan, V.A. Gupta, R. Majeti, and A. Weiss. 2005. The juxtamembrane wedge negatively regulates CD45 function in B cells. *Immunity.* 23:635–647.
23. Kishihara, K., J. Penninger, V.A. Wallace, T.M. Kundig, K. Kawai, A. Wakeham, E. Timms, K. Pfeffer, P.S. Ohashi, M.L. Thomas, et al. 1993. Normal B lymphocyte development but impaired T cell maturation in CD45-exon6 protein tyrosine phosphatase-deficient mice. *Cell.* 74:143–156.
24. Trowbridge, I.S., and M.L. Thomas. 1994. CD45: an emerging role as a protein tyrosine phosphatase required for lymphocyte activation and development. *Annu. Rev. Immunol.* 12:85–116.
25. Wright, D.E., S.H. Cheshier, A.J. Wagers, T.D. Randall, J.L. Christensen, and I.L. Weissman. 2001. Cyclophosphamide/granulocyte colony-stimulating factor causes selective mobilization of bone marrow hematopoietic stem cells into the blood after M phase of the cell cycle. *Blood.* 97:2278–2285.
26. Byk, T., J. Kahn, O. Kollet, I. Petit, S. Samira, S. Shivtiel, H. Ben-Hur, A. Peled, W. Piacibello, and T. Lapidot. 2005. Cycling G1 CD34+/CD38+ cells potentiate the motility and engraftment of quiescent G0 CD34+/CD38–/low severe combined immunodeficiency repopulating cells. *Stem Cells.* 23:561–574.
27. Fagerholm, S., T.J. Hilden, and C.G. Gahmberg. 2002. Lck tyrosine kinase is important for activation of the CD11a/CD18-integrins in human T lymphocytes. *Eur. J. Immunol.* 32:1670–1678.
28. Thomas, R.M., C. Schmedt, M. Novelli, B.K. Choi, J. Skok, A. Tarakhovsky, and J. Roes. 2004. C-terminal SRC kinase controls acute inflammation and granulocyte adhesion. *Immunity.* 20:181–191.
29. Lannutti, B.J., and J.G. Drachman. 2004. Lyn tyrosine kinase regulates thrombopoietin-induced proliferation of hematopoietic cell lines and primary megakaryocytic progenitors. *Blood.* 103:3736–3743.
30. Takamatsu, Y., P.J. Simmons, R.J. Moore, H.A. Morris, L.B. To, and J.P. Levesque. 1998. Osteoclast-mediated bone resorption is stimulated during short-term administration of granulocyte colony-stimulating factor but is not responsible for hematopoietic progenitor cell mobilization. *Blood.* 92:3465–3473.
31. Schwartzberg, P.L., L. Xing, O. Hoffmann, C.A. Lowell, L. Garrett, B.F. Boyce, and H.E. Varmus. 1997. Rescue of osteoclast function by transgenic expression of kinase-deficient Src in src−/− mutant mice. *Genes Dev.* 11:2835–2844.
32. Zhang, J., C. Niu, L. Ye, H. Huang, X. He, W.G. Tong, J. Ross, J. Haug, T. Johnson, J.Q. Feng, et al. 2003. Identification of the haematopoietic stem cell niche and control of the niche size. *Nature.* 425:836–841.
33. Gowen, M., F. Lazner, R. Dodds, R. Kapadia, J. Feild, M. Tavaria, I. Bertoncello, F. Drake, S. Zavarselk, I. Tellis, et al. 1999. Cathepsin K knockout mice develop osteopetrosis due to a deficit in matrix degradation but not demineralization. *J. Bone Miner. Res.* 14:1654–1663.
34. Walkley, C.R., J.M. Shea, N.A. Sims, L.E. Purton, and S.H. Orkin. 2007. Rb regulates interactions between hematopoietic stem cells and their bone marrow microenvironment. *Cell.* 129:1081–1095.
35. Asosingh, K., E. Menu, E. Van Valckenborgh, I. Vande Broek, I. Van Riet, B. Van Camp, and K. Vanderkerken. 2002. Mechanisms involved in the differential bone marrow homing of CD45 subsets in 5T murine models of myeloma. *Clin. Exp. Metastasis.* 19:583–591.
36. Roach, T., S. Slater, M. Koval, L. White, E.D. Cahir McFarland, M. Okumura, M. Thomas, and E. Brown. 1997. CD45 regulates Src family member kinase activity associated with macrophage integrin-mediated adhesion. *Curr. Biol.* 7:408–417.
37. Orschell, C.M., J. Borneo, V. Munugalavadla, P. Ma, E. Sims, B. Ramdas, M.C. Yoder, and R. Kapur. 2008. Deficiency of Src family kinases compromises the repopulating ability of hematopoietic stem cells. *Exp. Hematol.* 36:655–666.
38. Borneo, J., V. Munugalavadla, E.C. Sims, S. Vemula, C.M. Orschell, M. Yoder, and R. Kapur. 2007. Src family kinase-mediated negative regulation of hematopoietic stem cell mobilization involves both intrinsic and microenvironmental factors. *Exp. Hematol.* 35:1026–1037.
39. Lee, Y., A. Gotoh, H.J. Kwon, M. You, L. Kohli, C. Mantel, S. Cooper, G. Hangoc, K. Miyazawa, K. Ohyashiki, and H.E. Broxmeyer. 2002. Enhancement of intracellular signaling associated with hematopoietic progenitor cell survival in response to SDF-1/CXCL12 in synergy with other cytokines. *Blood.* 99:4307–4317.
40. Stier, S., Y. Ko, R. Forkert, C. Lutz, T. Neuhaus, E. Grunewald, T. Cheng, D. Dombkowski, L.M. Calvi, S.R. Rittling, and D.T. Scadden. 2005. Osteopontin is a hematopoietic stem cell niche component that negatively regulates stem cell pool size. *J. Exp. Med.* 201:1781–1791.
41. Nilsson, S.K., H.M. Johnston, G.A. Whitty, B. Williams, R.J. Webb, D.T. Denhardt, I. Bertoncello, L.J. Bendall, P.J. Simmons, and D.N. Haylock. 2005. Osteopontin, a key component of the hematopoietic stem cell niche and regulator of primitive hematopoietic progenitor cells. *Blood.* 106:1232–1239.
42. Delaisse, J.M., T.L. Andersen, M.T. Engsig, K. Henriksen, T. Troen, and L. Blavier. 2003. Matrix metalloproteinases (MMP) and cathepsin K contribute differently to osteoclastic activities. *Microsc. Res. Tech.* 61:504–513.
43. Ishibashi, O., S. Niwa, K. Kadoyama, and T. Inui. 2006. MMP-9 antisense oligodeoxynucleotide exerts an inhibitory effect on osteoclastic bone resorption by suppressing cell migration. *Life Sci.* 79:1657–1660.
44. Wan, Y., L.W. Chong, and R.M. Evans. 2007. PPAR-gamma regulates osteoclastogenesis in mice. *Nat. Med.* 13:1496–1503.
45. Mermel, C.H., M.L. McLemore, F. Liu, S. Pereira, J. Woloszynek, C.A. Lowell, and D.C. Link. 2006. Src family kinases are important negative regulators of G-CSF-dependent granulopoiesis. *Blood.* 108:2562–2568.
46. Abkowitz, J.L., A.E. Robinson, S. Kale, M.W. Long, and J. Chen. 2003. Mobilization of hematopoietic stem cells during homeostasis and after cytokine exposure. *Blood.* 102:1249–1253.

47. Jung, Y., J. Song, Y. Shiozawa, J. Wang, Z. Wang, B. Williams, A. Havens, A. Schneider, C. Ge, R.T. Franceschi, et al. 2008. Hematopoietic stem cells regulate mesenchymal stromal cell induction into osteoblasts thereby participating in the formation of the stem cell niche. *Stem Cells*. 26:2042–2051.
48. Bonig, H., G.V. Priestley, and T. Papayannopoulou. 2006. Hierarchy of molecular-pathway usage in bone marrow homing and its shift by cytokines. *Blood*. 107:79–86.
49. Agnihotri, R., H.C. Crawford, H. Haro, L.M. Matrisian, M.C. Havrda, and L. Liaw. 2001. Osteopontin, a novel substrate for matrix metalloproteinase-3 (stromelysin-1) and matrix metalloproteinase-7 (matrilysin). *J. Biol. Chem*. 276:28261–28267.
50. Hildebrand, T., A. Laib, R. Muller, J. Dequeker, and P. Ruegsegger. 1999. Direct three-dimensional morphometric analysis of human cancellous bone: microstructural data from spine, femur, iliac crest, and calcaneus. *J. Bone Miner. Res*. 14:1167–1174.